Fracture of Cr2O3 single crystals on the microscale

Materialia 15 (2021) 100961

Contents lists available at ScienceDirect

Materialia

journal homepage: www.elsevier.com/locate/mtla

Full Length Article

Fracture of Cr_2O_3 single crystals on the microscale

Anand H.S. Iyer, Krystyna Stiller, Magnus Hörnqvist Colliander*

Department of Physics, Chalmers University of Technology, 41296 Gothenburg, Sweden

ARTICLE INFO

Keywords:
Micromehanics
Electron microscopy
Fracture behavior
Ceramics
Chromia
Single crystal

ABSTRACT

Studying cleavage properties of protective oxide scales is imperative to understand their fracture behaviour, since transgranular fracture is observed in many cases. The small thickness and polycrystalline structure of such scales makes it difficult to identify active cleavage planes directly from mechanical testing. To resolve this issue for Cr_2O_3, we present an approach to experimentally identify cleavage planes through micro-cantilever bending. Single crystal wafers are used to prepare micro-cantilevers of pentagonal cross-section in different orientations, targeting possible cleavage planes. Fracture surface imaging showed rhombohedral and pyramidal fracture, though surface energy studies predict rhombohedral as the dominant plane. There does exist a preference for rhombohedral fracture over pyramidal, which is also revealed from the experiments.

1. Introduction

The integrity of oxide scales is crucial as their damage can affect the fatigue life of high temperature materials. Sites of oxide cracking and spallation can act as stress concentrators, thereby initiating cracks in the underlying material [1]. In order to develop physically based descriptions of the crack initiation process, mechanical properties such as elastic modulus, fracture toughness and fracture strain must be included [2–4]. These properties are, however, inherently difficult to measure due to the limited thickness of the oxide layers. Approaches such as resonance frequency method have been used in combination with acoustic emission to evaluate fracture in oxide scales [5,6]. Nanoindentation has also been very useful for estimation of hardness and elastic modulus of oxide scales [7,8]. But for thinner oxides scales, which are in the order of a few microns thick, such methods have limitations due to the influence of substrate material and residual stress effects [9]. A micro-cantilever geometry circumventing residual stresses and substrate effect was developed in order to study the fracture behaviour of sub-μm thermally grown oxide scales on a Ni-base superalloy [10]. The combination of extreme strain gradients in the thin scales and the presence of an outer cubic spinel on top of the inner Cr_2O_3 layer lead to the occurrence of pronounced plasticity and absence of oxide fracture in bending. In order to specifically investigate the fracture behaviour of the brittle Cr_2O_3, the same geometry was used in fracture testing of thermally grown Cr_2O_3 layers on pure Cr, at room temperature and 600°C [11]. Surprisingly, a significant amount of transgranular fracture occurred in these scales, even in the presence of strong stress concentrations created at the grain boundaries in the oxide layer. These results point to the need to understand the intragranular fracture behaviour of Cr_2O_3, in order to obtain a complete picture of the oxide failure process. As there is very limited information regarding cleavage of Cr_2O_3 available in the literature, and existing reports are based on simulations of surface energies [12,13] or on commonly occurring cleaved planes in minerals [14], an attempt was made to identify the fracture planes in the oxide cantilevers in [11]. This is, however, very challenging due to the small grain size, heterogeneous microstructure and presence of defects. This calls for testing of single crystals in order to avoid issues such as heterogeneity and presence of defects. Single crystal fracture toughness measurements on the microscale have been conducted on Al_2O_3 [15], showing smooth and flat fracture surface for prismatic planes and faceted fracture for basal plane, but much less is known regarding the fracture behaviour of Cr_2O_3. Prior studies of fracture behaviour of Cr_2O_3 on the microscale have been conducted using microhardness fracture toughness testing on polycrystalline specimens, either in sintered form or as layered Cr_2O_3/Cr coatings obtained by physical vapour deposition (PVD) [16–18].

Schultz et al. [19] suggested a fracture toughness based criterion to determine preferential cleavage, where they explain that the lowest plane specific fracture toughness reveals the cleavage plane. Computer simulation studies on various systems also suggest planes with lowest relaxed surface energy as the preferred cleavage planes [12,13]. Di Maio et al. [20] proposed a micro-cantilever based geometry for fracture toughness evaluation, in which a FIB milled notch is used to initiate fracture. This has since then been extensively used in microscale fracture toughness evaluation of several materials [15,21–24] and the state-of-the-art is reviewed in [25,26]. The method also provides the freedom of preparation of cantilevers in different crystallographic orientations enabling the evaluation of plane specific fracture toughness which has

* Corresponding author.
E-mail address: magnus.colliander@chalmers.se (M. Hörnqvist Colliander).

https://doi.org/10.1016/j.mtla.2020.100961
Received 2 July 2020; Accepted 14 November 2020
Available online 18 November 2020

been performed for many material systems, including oxides such as Al_2O_3 [15] and cubic ZrO_2 [24]. However, no plane specific trend has been observed in these studies that could explain preferential cleavage. Micro-pillar splitting is another technique that has been used in fracture toughness measurement that can circumvent the effects of FIB damage, which affects the measured values in micro-cantilever bending [27,28]. But, this method does not allow the targeting of crystallographic planes as it is based on cracks generated from indentation of a controlled volume of material. There are also other alternative geometries including clamped cantilever bending [29], double cantilever beam compression [30] and double cantilever wedge splitting [31]. Cantilever bending and pillar splitting, however, have emerged as the dominating methods due to the ease and flexibility of specimen preparation and straightforward analysis and interpretation.

In this work, we perform microscale fracture tests of single crystal Cr_2O_3, targeting different potential fracture planes. The target planes were chosen on the basis of potential cleavage planes observed in Cr_2O_3 from surface energy simulations [12], and also from experimental evidence seen in other corundum oxides such as Al_2O_3 [15,32,33]. We use the approach of testing unnotched cantilevers to identify favourable cleavage planes for Cr_2O_3, since it allows for competition between different potential fracture planes, thus identifying naturally occurring weak orientations. The use of microscale testing ensures that the probed volume is small, and thus unlikely to contain any defects which can initiate fracture. Additionally, micro-pillar splitting tests are performed to understand cleavage when no specific planes are targeted. The results provide new insights into the microscale fracture behaviour of Cr_2O_3, in particular the crystallographic nature of transgranular fracture.

2. Materials and methods

In order to allow targeting of all intended crystallographic planes, Cr_2O_3 single crystal wafers with two difference orientations – {0001} and {1120} – were purchased from MaTecK GmbH, Germany. The wafers were grown by the Verneuil process and had dimensions $5 \times 5 \times 0.1$ mm. The same wafers were used for all studies, including micro-pillar splitting.

2.1. Micro-cantilever preparation

Surface micro-cantilevers of pentagonal cross-section (Fig. 1(c)) with the tensile axis perpendicular to the targeted plane (Fig. 1(a)) were prepared in a FEI Versa3D FIB-SEM. Pentagonal cross-section, which is typically used for fracture toughness testing of notched micro-cantilevers [20,21] was chosen in the current case to facilitate the identification of fractured planes through imaging from the sides (which is difficult for triangular cross-section). Electron back-scatter diffraction (EBSD) was performed on the wafers to determine the in-plane orientation with respect to the edges of the specimen to enable the preparation of micro-cantilevers in the targeted orientations. The deviation from ideal orientation was measured to be $< 3^\circ$ for the {0001} wafer and $< 1^\circ$ for {1120} wafer arising mainly due to mounting of the wafer on the Al stub used as sample holder during microscopy. The targeted planes were the $m\{10\bar{1}0\}$, $a\{11\bar{2}0\}$, $p\{10\bar{1}1\}$, $r\{10\bar{1}2\}$, $c\{0001\}$ planes and a high index plane 45° to the m plane (on the {0001} wafer), see Fig. 1. Two cantilevers for each orientation were prepared. The naming was in accordance with the targeted plane of fracture, as shown in Fig. 1(a). As the m plane was targeted in both wafers, we use m to denote cantilevers in the {0001} wafer and m′ to denote cantilevers in the {1120} wafer. The initial rough milling was performed using currents of 5–7 nA and the final polishing was done using a lower current of 300 pA to remove the redeposited layers and to obtain the expected geometry. An overtilt of 1.5° was used for the final milling steps in order to account for the profile of the ion beam. The beam energy for all steps was 30 keV. The actual orientation of each cantilever relative to the intended target plane was checked using EBSD after milling, and the deviation from the orientation was typically $< 1.5^\circ$. The prepared cantilevers were imaged in a Zeiss Ultra55 FEG SEM from the top and sides to measure the dimensions (see supplementary material section A for dimensions of all cantilevers).

2.2. Micro-pillar preparation

Micro-pillars for pillar splitting experiments were also prepared using the same FIB instrument. The pillars were prepared by annular milling with a beam energy of 30 keV and an initial current of 1 nA to create the approximate shape of desired depth. The final polishing was performed in two steps with 100 pA and 50 pA currents to reduce the taper. A taper of $< 3^\circ$ was obtained through these milling steps. Between each step, the sample was rotated in order to avoid asymmetry in the shape of the pillar. A marker was milled at the centre of the pillar with a current of 10 pA to guide tip placement. The pillar diameter, D, was roughly 2 μm in most cases and the height, h, was slightly more than 2 μm conforming to the recommendation of D/h around 1 [22,27]. Nine pillars were prepared on each wafer.

2.3. Micromechanical testing

The mechanical tests were performed using an Alemnis in-situ nanoindenter setup (Alemnis AG, Switzerland) in a Zeiss Ultra55 FEG SEM using a cono-spherical diamond tip of radius 1 μm. The fracture tests were conducted in displacement control mode at 20 nm s^{-1}, and the indenter tip was withdrawn at fracture. The raw force displacement data obtained is corrected for load drift and thermal drift, which is measured separately for each cantilever. The system compliance is considered as well in displacement corrections. At higher loads nearing fracture, the indentation effect of the tip cannot be neglected, so a fitted function from indentation on bulk surface is used to correct for the displacement due to indentation for the cantilevers [34]. The fracture surfaces were imaged in a Tescan GAIA3 FIB-SEM to measure the fracture angles.

For the micro-pillar splitting, the fracture tests were conducted in the displacement mode with proportional displacement at the rate of 0.05 nm s^{-1} using a cube corner indenter. The cube corner geometry was chosen to enable easy alignment of tip with pillar centre. To test the influence of tip orientation on fracture of pillars, the sample was tested in three different orientations with respect to the tip (Fig. 2). Three pillars were tested in each orientation.

3. Results

3.1. Micro-cantilevers

In total 14 cantilevers (7 orientations, two tests per orientation) were tested to fracture. From the force-displacement curves (shown in supplementary material section B), it was seen that the fracture behaviour was elastic. The orientation of the different potential cleavage planes was calculated with the help of c/a ratio of Cr_2O_3, as shown in Fig. 3. Secondary electron imaging of the tested cantilevers was used to identify the fracture planes through matching of the resulting fracture surface to the traces of the different potential planes. Note that the images in Figs. 4 and 5 were acquired at a tilt of 70°, and the numbers associated with the angles indicated are tilt corrected. The unit cell is superimposed on the images to demonstrate how the cleavage planes have been determined and also to visualise the plane. The drawn traces are not corrected and only show approximate relationships with the schematic unit cell. However, the tilt correction is small (~5%) so the approximation is sufficient for visual correlation between unit cells and fracture surface angles. Here we show only selected representative cantilevers, but the images of all the fractured cantilevers can be found in supplementary material section C.

In the case of {0001} wafer, the m-cantilevers showed pyramidal cleavage (Fig. 4(a)), a-cantilevers showed rhombohedral cleavage

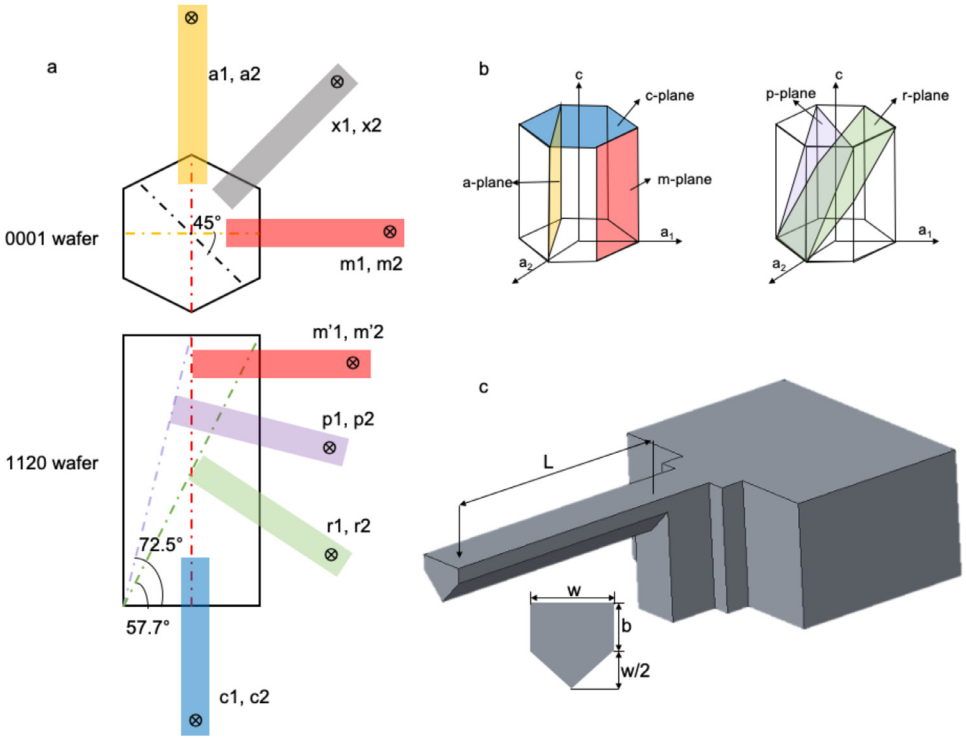

Fig. 1. (a) Schematic showing orientations of tested cantilevers; (b) Orientation of targeted planes shown in unit cell; (c) cantilever geometry with pentagonal cross-section.

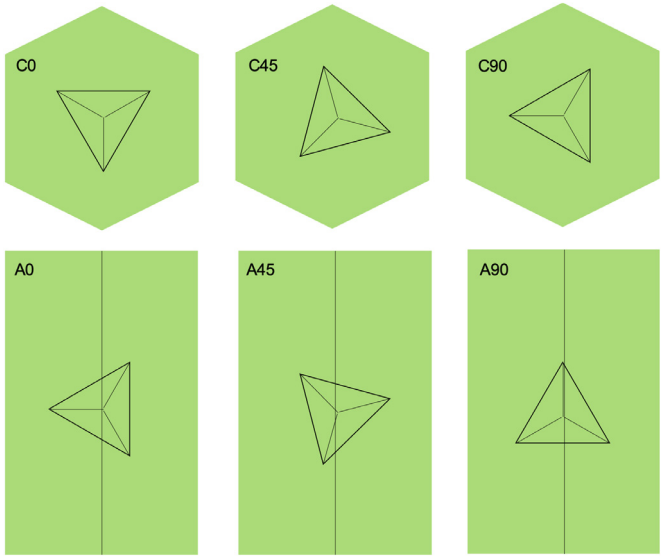

Fig. 2. Schematic showing the strategy for testing different orientations. The naming conventions for each condition is shown as well. The {0001} wafer is named as C, and {1120} as A.

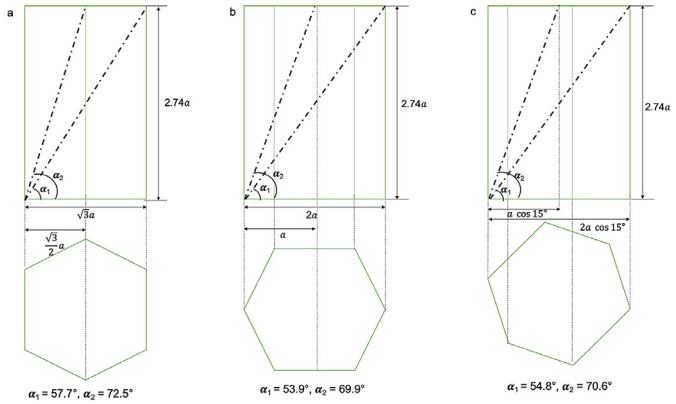

Fig. 3. Diagrams of unit cell showing how angles are calculated for (a) *m* cantilever orientation; (b) *a* cantilever orientation; and (c) *x* cantilever orientation.

Table 1
Fracture planes for tested micro-cantilevers.

Sample	Targeted plane	Fracture plane
m1, m2	*m*	*p*
x1, x2	-	*p+r*
a1, a2	*a*	*r*
c1, c2	*c*	*unknown*
p1, p2	*p*	*r*
r1, r2	*r*	*r*
m′1, m′2	*m*	*p+unknwon*

(Fig. 4(c)), and the x-cantilevers show fracture along both these two planes (Fig. 4(b)). In the case of c-cantilevers in the {1120} wafer, one of them did not show a clear cleavage plane and the angles of cleavage of the other did not correspond to the either of the above cleavage planes. This is consistent with observations of fracture in *c*-oriented alumina cantilevers, where complex facetted fracture was observed instead of cleavage [15]. The m′-cantilevers showed pyramidal fracture, similar to that of m. However, the two m′-cantilevers had a fracture surface consisting of two intersecting planes, one of which corresponded to *p* plane but the other did not align with any known cleavage plane (Fig. 5(a)). Surprisingly, *p*-oriented cantilevers showed fracture in the *r* plane rather than the pyramidal (Fig. 5(b)), whereas the ones oriented with *r* plane perpendicular to the tensile axis showed cleavage along that plane (Fig. 5(c)). The cleavage behaviour of Cr_2O_3 observed from the experiments have been summarised in Table 1.

The fracture surfaces show features such as cleavage steps even though the fracture seems to follow the aforementioned cleavage planes. Fig. 6 shows the fracture surfaces for different cantilevers. Fig. 6(c)

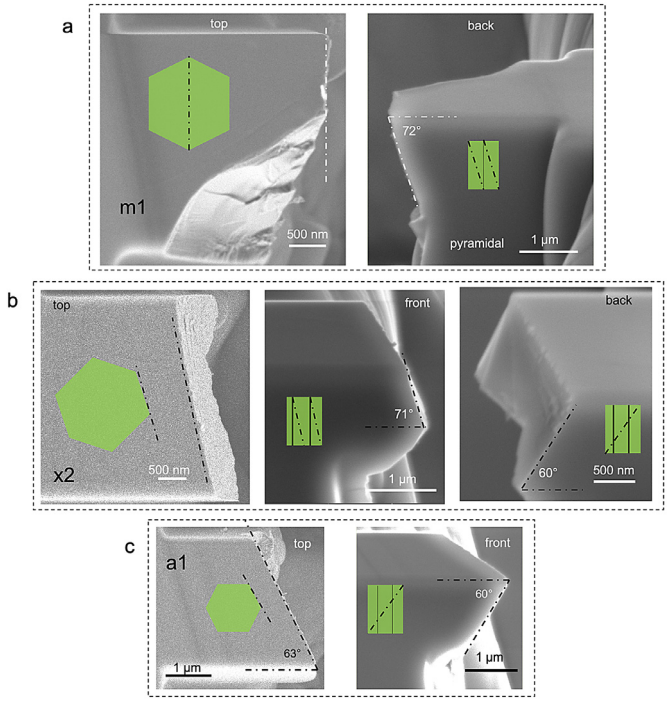

Fig. 4. Top and side view SEM images of tested micro-cantilevers on the {0001} wafer with the unit cell overlapped revealing planes of fracture which is pyramidal in (a), mixed pyramidal + rhombohedral in (b) and rhombohedral in (c).

shows clear cleavage steps, while for cantilever x2 in Fig. 6(b), two different cleavage planes can be seen. For the m-cantilevers, conchoid like fracture extending into the support was seen as well along with pyramidal cleavage, which can be seen from Figs. 4(a) and 6(a).

3.2. Micro-pillars

In order to evaluate how cleavage occurs without targeting a certain crystallographic plane, micro-pillar splitting experiments were performed. Nine pillars with three different orientations (see Fig. 2) on each wafer were successfully tested. In all cases, only two branches of cracks originated from the indent. The third crack branch initiated for some pillars due to further downward movement of the tip after the first cracking. For pillars tested on {0001} wafer, the splitting seems to be along the sharp edges of the indenter (Fig. 7(a)), regardless of tip orientation, whereas the cracks in {1120} pillars showed cleavage along the rhombohedral plane, as demonstrated in Fig. 7(b) with the superposed unit cell. The crack seems to divide the pillar in half and the splitting does not occur along the sharp indenter edges.

4. Discussion

The fracture of tested single crystal Cr_2O_3 cantilevers provides an insight into its preferential cleavage planes. The images of the fractured cantilevers of different orientation clearly show that fracture on the rhombohedral and pyramidal planes dominates. Rhombohedral appears to be favoured over pyramidal since fracture along this plane occurs even in cantilevers specifically oriented to target pyramidal planes. This is seen from the micro-pillar tests as well where all pillars on the {1120} wafer cleaved along the rhombohedral plane. In no case fracture along the *m* or *a* planes, sometimes seen in grown single crystals of alumina [32], was observed. In the previous work [11], only traces of *a* and *m* plane were compared to the crack direction, basing the assumption on alumina cleavage planes. Since the comparison was performed based on plane traces, it would have been difficult to distinguish between *p, r* and *m* plane since the traces would be parallel.

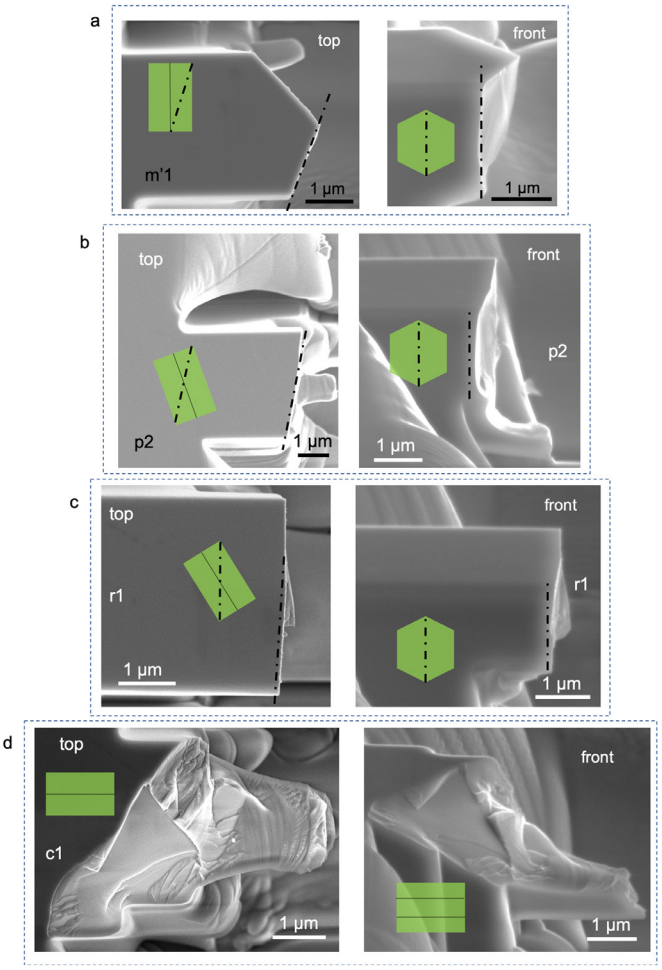

Fig. 5. Fracture surfaces of tested micro-cantilevers on {1120} wafer; (a) pyramidal cleavage in m′-cantilever; (b) rhombohedral cleavage in p-cantilever; (c) rhombohedral cleavage in r-cantilever; and (d) undefined cleavage fracture in c-cantilever.

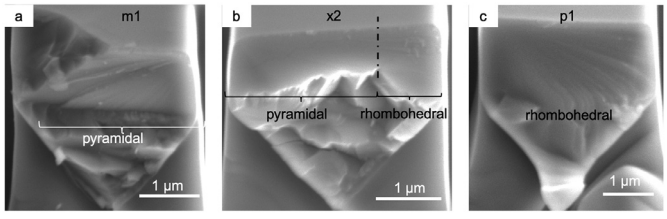

Fig. 6. Fracture surfaces of (a) m1 showing pyramidal cleavage; (b) x2 showing mixed pyramidal and rhombohedral cleavage; and (c) p1 showing rhombohedral cleavage.

The observation of rhombohedral cleavage is well in agreement with various literature studies on simulations of surface energies of different planes of Cr_2O_3, where the rhombohedral $\{10\bar{1}2\}$ plane shows the lowest relaxed surface energy [12,13]. Also, in the corundum structure, the empty octahedral sites are arranged in this plane, thus facilitating easy cleavage [14]. However, for m and m′-cantilevers, pyramidal $\{10\bar{1}1\}$ cleavage was seen as well, even though the relaxed surface energy difference is much higher for this plane (equal to or higher than both *m* and *a* plane) [12,13] and it has not been previously reported for Cr_2O_3. For both *m* and *m′* cantilevers the pyramidal plane is closer to being perpendicular to the tensile axis compared to the rhombohedral plane, indicating that there is likely a geometric effect. One of the studies on cleavage

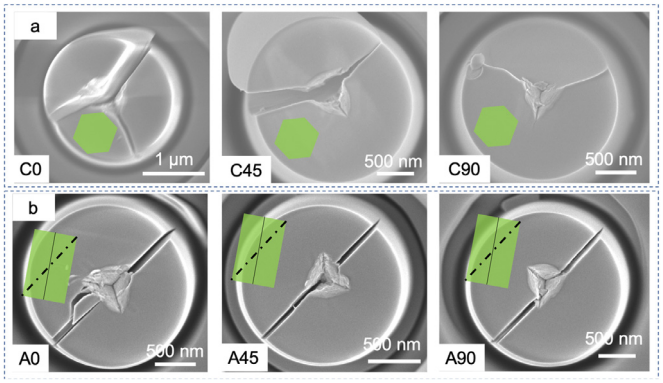

Fig. 7. SEM images of fractured pillars with unit cell overlapped.

of alumina [33] mentions pyramidal cleavage, which is attributed to the parallel planes of large anions and larger distance between them.

In the case of the fracture surfaces of the tested cantilevers (Fig. 6), the bottom part does not show a clean cleavage, which can be a result of the complex stress state and change in geometry of the pentagonal cross-section. A rectangular or square cross-section can solve these issues, but for this geometry it is not possible to target specific orientations unless individual wafers with ideal in-plane orientation aligned with the wafer edges are used for making cantilevers close to the edge. Even in the present geometry, the alignment of the crystallographic planes is not exact. EBSD is performed to identify the amount of rotation of the wafer required to make cantilevers in different orientations, but errors in stage rotation and EBSD leads to small misalignments $< 1^{\circ}$. This results in some discrepancies in the measured angles of fracture, but it is considered negligible in this case. Similarly, the deviation from ideal orientation of the wafer growth axis with the vertical direction ($< 3^{\circ}$) due to mounting can be neglected.

The experimental approach shown in this work is powerful in determination of preferential cleavage in such systems, which can also be used as validation for computer simulation studies. The use of single crystals provide more control over the orientations that can be tested, but it is possible to utilise the same approach in studying cleavage, as has been done in some cases [15,24]. As mentioned before, such an in depth study on transgranular fracture has implications with regard to explaining the fracture behaviour of protective oxide scales in high temperature materials and also for textured coatings, and can aid in design improvements based on the gained knowledge. We also note that the methodology developed herein would be possible to apply also on polycrystalline materials, provided that sufficiently large grains with suitable orientations could be identified.

5. Conclusions

Using bending of micro-cantilevers along different crystallographic planes, cleavage in Cr_2O_3 has been investigated. Rhombohedral $\{10\bar{1}2\}$ and pyramidal $\{10\bar{1}1\}$ planes have been shown to be the preferential cleavage planes. Among these two planes, a slight preference seems to exist for rhombohedral fracture, revealed by rhombohedral fracture of micro-cantilevers oriented perpendicular to pyramidal plane and also the fracture of micro-pillars on $\{1120\}$ wafer. While cleavage along the rhombohedral plane was not unexpected due to the low relaxed surface energy, pyramidal fracture cannot be explained by energetic arguments.

Declaration of Competing Interest

The authors declare that they have no known competing financial interests or personal relationships that could have appeared to influence the work reported in this paper.

Acknowledegements

The authors would like to acknowledge the research funding from Vetenskapsrådet (Swedish Research Council) grant number 2015-04719. The experiments were conducted at Chalmers Materials Analysis Laboratory (CMAL), Gothenburg, Sweden.

Supplementary materials

Supplementary material associated with this article can be found, in the online version, at doi:10.1016/j.mtla.2020.100961.

References

[1] S. Cruchley, H.Y. Li, H.E. Evans, P. Bowen, D.J. Child, M.C. Hardy, The role of oxidation damage in fatigue crack initiation of an advanced Ni-based superalloy, Int. J. Fatigue 81 (2015) 265–274, doi:10.1016/j.ijfatigue.2015.08.016.
[2] M. Schütze, P.F. Tortorelli, I.G. Wright, Development of a comprehensive oxide scale failure diagram, Oxid. Met. 73 (2010) 389–418, doi:10.1007/s11085-009-9185-7.
[3] M. Schütze, Modelling oxide scale fracture, Mater. High Temp. 22 (2005) 147–154, doi:10.1179/mht.2005.017.
[4] M. Schütze, W.J. Quadakkers, Future directions in the field of high-temperature corrosion research, Oxid. Met. 87 (2017) 681–704, doi:10.1007/s11085-017-9719-3.
[5] M. Schutze, S. Ito, W. Przybilla, H. Echsler, C. Bruns, Test methods and data on the mechanical properties of protective oxide scales, Mater. High Temp. 18 (2001) 39–50, doi:10.1179/mht.2001.004.
[6] J.R. Nicholls, C. Mendes, P. Hancock, Measurement methods to determine the elastic properties of oxides at elevated temperatures, Mater. High Temp. 12 (1994) 85–94, doi:10.1080/09603409.1994.11689473.
[7] P.F. Tortorelli, S.R.J. Saunders, G. Shafirstein, D.J. Hall, Use of the mechanical properties microprobe for characterization of oxide scales, Mater. High Temp. 12 (1994) 95–101, doi:10.1080/09603409.1994.11689474.
[8] P.F. Tortorelli, Mechanical properties of chromia scales, Le J. Phys. IV 03 (1993) C9-943-C9-949. doi:10.1051/jp4:1993997.
[9] M.M. Nagl, W.T. Evans, S.R.J. Saunders, D.J. Hall, Investigation of failure of brittle layers under compressive stresses using acoustic emission, Mater. Sci. Technol. 8 (1992) 1043–1050, doi:10.1179/mst.1992.8.11.1043.
[10] A.H.S. Iyer, K. Stiller, M.H. Colliander, Room temperature plasticity in thermally grown sub-micron oxide scales revealed by micro-cantilever bending, Scr. Mater. 144 (2018) 9–12, doi:10.1016/j.scriptamat.2017.09.036.
[11] A.H.S. Iyer, G. Mohanty, K. Stiller, J. Michler, M.H. Colliander, Microscale fracture of chromia scales, Materialia 8 (2019) 100465, doi:10.1016/j.mtla.2019.100465.
[12] P.J. Lawrence, S.C. Parker, P.W. Tasker, Computer simulation studies of perfect and defective surfaces in Cr_2O_3, J. Am. Ceram. Soc. 71 (1988) C-389-C–391, doi:10.1111/j.1151-2916.1988.tb06401.x.
[13] J. Sun, T. Stirner, A. Matthews, Structure and surface energy of low-index surfaces of stoichiometric α-Al_2O_3 and α-Cr_2O_3, Surf. Coatings Technol. 201 (2006) 4205–4208, doi:10.1016/j.surfcoat.2006.08.061.
[14] V.E. Henrich, P.A. Cox, The Surface Science of Metal Oxides, Cambridge University Press, 1994.
[15] A.D. Norton, S. Falco, N. Young, J. Severs, R.I. Todd, Microcantilever investigation of fracture toughness and subcritical crack growth on the scale of the microstructure in Al_2O_3, J. Eur. Ceram. Soc. 35 (2015) 4521–4533, doi:10.1016/j.jeurceramsoc.2015.08.023.
[16] X. Pang, K. Gao, F. Luo, Y. Emirov, A.A. Levin, A.A. Volinsky, Investigation of microstructure and mechanical properties of multi-layer Cr/Cr_2O_3 coatings, Thin Solid Films 517 (2009) 1922–1927, doi:10.1016/j.tsf.2008.10.026.
[17] K. Shibata, M. Yoshinaka, K. Hirota, O. Yamaguchi, Fabrication and mechanical properties of Cr_2O_3 solid solution ceramics in the system Cr_2O_3-Al_2O_3, Mater. Res. Bull 32 (1997) 627–632, doi:10.1016/S0025-5408(97)00015-9.
[18] J. Li, Y. Zhang, J. Huang, C. Ding, Mechanical and tribological properties of plasma-sprayed Cr_3C_2 -NiCr, WC-Co, and Cr_2O_3 coatings, J. Therm. Spray Technol. 7 (1998) 242–246.
[19] R.A. Schultz, M.C. Jensen, R.C. Bradt, Single crystal cleavage of brittle materials, Int. J. Fract. 65 (1994) 291–312, doi:10.1007/BF00012370.
[20] D. Di Maio, S.G.G. Roberts, Measuring fracture toughness of coatings using focused-ion-beam-machined microbeams, J. Mater. Res. 20 (2005) 299–302, doi:10.1557/JMR.2005.0048.
[21] D.E.J. Armstrong, A.J. Wilkinson, S.G. Roberts, Micro-mechanical measurements of fracture toughness of bismuth embrittled copper grain boundaries, Philos. Mag. Lett. 91 (2011) 394–400, doi:10.1080/09500839.2011.573813.
[22] B.N. Jaya, C. Kirchlechner, G. Dehm, Can microscale fracture tests provide reliable fracture toughness values? A case study in silicon, J. Mater. Res. 30 (2015) 686–698, doi:10.1557/jmr.2015.2.
[23] J. Ast, M.N. Polyakov, G. Mohanty, J. Michler, X. Maeder, Interplay of stresses, plasticity at crack tips and small sample dimensions revealed by in-situ microcantilever tests in tungsten, Mater. Sci. Eng. A 710 (2018) 400–412, doi:10.1016/j.msea.2017.10.096.
[24] R. Henry, T. Blay, T. Douillard, A. Descamps-Mandine, I. Zacharie-Aubrun, J.-M. Gatt, C. Langlois, S. Meille, Local fracture toughness measurements in polycrystalline cubic zirconia using micro-cantilever bending tests, Mech. Mater. 136 (2019) 103086, doi:10.1016/j.mechmat.2019.103086.

[25] J. Ast, M. Ghidelli, K. Durst, M. Göken, M. Sebastiani, A.M. Korsunsky, A review of experimental approaches to fracture toughness evaluation at the micro-scale, Mater. Des. 173 (2019) 107762, doi:10.1016/j.matdes.2019.107762.
[26] M. Sebastiani, K.E. Johanns, E.G. Herbert, G.M. Pharr, Measurement of fracture toughness by nanoindentation methods: Recent advances and future challenges, Curr. Opin. Solid State Mater. Sci. (2015), doi:10.1016/j.cossms.2015.04.003.
[27] M. Sebastiani, K.E. Johanns, E.G. Herbert, F. Carassiti, G.M. Pharr, A novel pillar indentation splitting test for measuring fracture toughness of thin ceramic coatings, Philos. Mag. 95 (2015) 1928–1944, doi:10.1080/14786435.2014.913110.
[28] M. Ghidelli, M. Sebastiani, K.E. Johanns, G.M. Pharr, Effects of indenter angle on micro-scale fracture toughness measurement by pillar splitting, J. Am. Ceram. Soc. 100 (2017) 5731–5738, doi:10.1111/jace.15093.
[29] N. Jaya B, V. Jayaram, S.K. Biswas, A new method for fracture toughness determination of graded (Pt,Ni)Al bond coats by microbeam bend tests, Philos. Mag. 92 (2012) 3326–3345, doi:10.1080/14786435.2012.669068.
[30] S. Liu, J.M. Wheeler, P.R. Howie, X.T. Zeng, J. Michler, W.J. Clegg, Measuring the fracture resistance of hard coatings, Appl. Phys. Lett. 102 (2013) 171907, doi:10.1063/1.4803928.
[31] G. Sernicola, T. Giovannini, P. Patel, J.R. Kermode, D.S. Balint, T. Ben Britton, F. Giuliani, In situ stable crack growth at the micron scale, Nat. Commun. 8 (2017), doi:10.1038/s41467-017-00139-w.
[32] V. Pishchik, L.A. Lytvynov, E.R. Dobrovinskaya, Sapphire, Springer US, Boston, MA, 2009, doi:10.1007/978-0-387-85695-7.
[33] H.S. Bagdasarov, G.V. Berezhkova, V.G. Govorkov, E.P. Kozlovskaya, E.A. Fedorov, M.A. Chernysheva, The geometry of fractures caused by cleavage of α-Al_2O_3 single crystals, Krist. Und Tech. 8 (1973) 507–511, doi:10.1002/crat.19730080414.
[34] D. Kupka, E.T. Lilleodden, Mechanical testing of solid-solid interfaces at the microscale, Exp. Mech. (2012), doi:10.1007/s11340-011-9530-z.